Understanding Cooperativity in Hydrogen-Bond-Induced Supramolecular Polymerization: A Density Functional Theory Study

Ivo A. W. Filot,[†,‡] Anja R. A. Palmans,[†,§] Peter A. J. Hilbers,[†,||] Rutger A. van Santen,[†,‡] Evgeny A. Pidko,*[,†,‡] and Tom F. A. de Greef*[,†,||]

Institute for Complex Molecular Systems, Schuit Institute of Catalysis, Laboratory of Macromolecular and Organic Chemistry, and Department of Biomedical Engineering, Eindhoven University of Technology, P.O. Box 513, 5600 MB, Eindhoven, The Netherlands

Received: August 3, 2010; Revised Manuscript Received: September 20, 2010

Understanding the molecular mechanism of cooperative self-assembly is a key component in the design of self-assembled supramolecular architectures across multiple length scales with defined function and composition. In this work, we use density functional theory to rationalize the experimentally observed cooperative growth of C_3-symmetrical trialkylbenzene-1,3,5-tricarboxamide- (BTA-) based supramolecular polymers that self-assemble into ordered one-dimensional supramolecular structures through hydrogen bonding. Our analysis shows that the cooperative growth of these structures is caused by electrostatic interactions and nonadditive effects brought about by redistribution of the electron density with aggregate length.

Introduction

The hierarchical self-assembly of organic molecules into micro- and nanoscopic one-dimensional (1D) objects such as fibers, rods, and whiskers using well-defined noncovalent forces has recently gained considerable attention as a technique for the fabrication of functional structures, such as biologically active structures for biomedical functions[1−3] and π-conjugated wires[4−6] for use in organic waveguides,[7] n-channel transistors,[8] and phototransistors.[9] The diverse applications of one-dimensional supramolecular architectures demand a precise understanding of the interplay between growth of the supramolecular structures at each level of the assembly process and the noncovalent interactions responsible for their formation. In many cases, the first stage of a hierarchical self-assembly process consists of the noncovalent association of monomers into a 1D supramolecular polymer, followed by chain bundling as a result of weaker interactions at higher concentrations.[10−14] Therefore, uncovering the critical features that dictate the growth from monomer to supramolecular polymer is a requirement for the bottom-up fabrication of hierarchical self-assembled 1D supramolecular structures across multiple length scales with defined function and composition.

Recently, three distinct growth mechanisms of one-dimensional supramolecular polymers, namely, isodesmic, ring−chain, and growth through a cooperative mechanism, were defined.[15,16] In an isodesmic supramolecular polymerization, the binding of each new monomer to the growing chain is independent of the length of the chain. This mechanism implies that the energy per monomer in a supramolecular polymer is independent of the degree of aggregation, that is, that the interaction energies are additive. In contrast to the isodesmic growth mechanism, cooperative growth is characterized by an enhanced propensity for monomer addition as the number of monomers in the chain increases. From an energetic point of view, cooperativity is defined as a nonadditive property of interacting monomers, as the interaction energy per monomer depends on the degree of aggregation.[17]

The cooperative growth of supramolecular polymers can be classified into three different types: cooperativity arising from electronic effects, structural features (both helix formation and allosteric conformational changes), or the hydrophobic effect.[15] Strong electronic cooperativity is frequently encountered in artificial and biological supramolecular systems where hydrogen bonding is the dominant noncovalent interaction between individual subunits.[18−27] Dannenberg and co-workers reported extensive Hartree−Fock (HF), density functional theory (DFT), and second-order Møller−Plesset perturbation theory (MP2) calculations on linear hydrogen-bonded systems consisting of linear chains of urea[28,29] and formamide[30,31] molecules. A cooperative effect of almost 200% of the dimer interaction energy operating in long hydrogen-bonded formamide[30] chains was found, whereas for hydrogen-bonded urea[29] chains, this value was much lower (46%).[30] They attributed[30] the unusually large cooperative hydrogen bonding in formamide chains to the following electronic effects: (1) pairwise electrostatic interactions (mainly long-range dipole−dipole interactions), (2) nonpairwise short-range (mutual) polarization, and (3) resonance-assisted hydrogen bonding.[32,33] In the last two cases, the strength of the hydrogen bonds increases as a result of the redistribution of the electron density along the chain. Using a pairwise model for the long-range dipole−dipole interactions, the contribution of nonpairwise electronic interactions to the total hydrogen-bond cooperativity was estimated to be as high as 75%.[31] More recent DFT calculations by Baker and co-workers[34] on the cooperativity of hydrogen-bond interactions in a model system for α-helix formation have shown that nonpairwise electronic effects account for half of the total cooperativity that is observed in this system.

To understand the origin of cooperativity in supramolecular polymerizations, we set out to study the self-assembly mechanism of supramolecular polymers in dilute solutions having a wide range of different structure-directing noncovalent interac-

* Corresponding authors. E-mail: e.a.pidko@tue.nl (E.A.P.), t.f.a.d.greef@tue.nl (T.F.A.d.G.).
[†] Institute for Complex Molecular Systems.
[‡] Schuit Institute of Catalysis.
[§] Laboratory of Macromolecular and Organic Chemistry.
[||] Department of Biomedical Engineering.

10.1021/jp1072928
Published on Web 10/13/2010

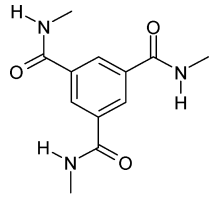

1

Figure 1. Structural formula of BTA monomer **1**.

tions between the monomeric units.[35] In particular, we investigated in detail the supramolecular polymerization of chiral C_3-symmetrical trialkylbenzene-1,3,5-tricarboxamides (BTAs), which self-assemble in dilute apolar solutions through threefold amide-type hydrogen bonding,[36−38] using temperature-dependent spectroscopic techniques.[39] The nonsigmoidal melting curves obtained by temperature-dependent UV−visible and circular dichroism (CD) measurements on dilute BTA solutions are indicative of a cooperative supramolecular growth mechanism[40] and could be analyzed using a recently proposed thermodynamic model for thermally activated equilibrium polymerizations.[41] The directionality and strong association of BTA monomers into ordered hydrogen-bonded columns has been used to construct supramolecular materials,[42] organogelators,[43,44] and liquid-crystalline materials.[45] Furthermore, the helical order of the BTA columns has been shown to be beneficial in the nucleation of isotactic polypropylene.[46] However, the molecular basis of the observed cooperativity in BTAs remains unclear.

Herein, we rationalize the experimentally found large degrees of cooperativity in the hydrogen-bond-mediated supramolecular polymerization of C_3-symmetrical trialkylbenzene-1,3,5-tricarboxamides using density functional theory (DFT) calculations. Plane-wave (PW) DFT calculations were performed on hydrogen-bonded BTA chains containing up to seven monomers, and several characteristics, such as bond length, bond strength, and dihedral angles, were compared as a function of chain length. The results of this theoretical study highlight the importance of electronic effects in the formation of highly ordered hydrogen-bonded supramolecular assemblies.

Computational Details

To reduce computational costs, calculations were performed on oligomers and the infinite chain of BTA monomer **1** (Figure 1) in which the long aliphatic tails used in the experimental studies were replaced by a methyl group.[39] Plane-wave DFT (PW-DFT) electronic-structure calculations were performed for the monomer up to and including the heptamer using the Vienna ab initio simulation package (VASP).[47,48] All DFT calculations were performed using the Perdew−Becke−Ernzerhof (PBE)[49] exchange-correlation functional. The projector-augmented wave (PAW)[50,51] method was used to describe electron−ion interactions, and for valence electrons, a plane-wave basis set was employed. The energy cutoff was set to 400 eV (see the Supporting Information). The Brillouin zone sampling was restricted to the Γ point. The PBE functional has previously been shown to accurately describe hydrogen-bond-dominated as well as mixed (hydrogen bond and dispersion) molecular systems using both plane waves and localized orbitals.[52−60] In contrast, it has been shown that the PBE functional gives large mean errors for the interaction energies of dispersion-dominated complexes (i.e., noncovalent complexes dominated by $\pi-\pi$ or van der Waals interactions).[59,61] However, recent DFT, MP2, and coupled-cluster with single and double and perturbative triple excitations [CCSD(T)] calculations have shown that the interaction energy of formamide-type hydrogen bonds such as those found in chains of **1** is roughly 6 times larger than the interaction energy of stacked benzene dimers that are dominated by $\pi-\pi$ interactions.[59,62−64] Because other dispersion effects (such as van der Waals interactions) are even weaker than $\pi-\pi$ interactions,[59,63] the formation of three hydrogen bonds implies that the formation of one-dimensional chains of **1** is mainly governed by hydrogen bonds. Furthermore, high-level MP2 calculations have shown that $\pi-\pi$ interactions in simple sandwich-type benzene stacks are additive and, therefore, will not contribute significantly to the experimentally observed large degrees of cooperativity.[65]

Monomer and oligomers of **1** were placed in an ($a \times a \times c$) orthorhombic supercell. A sufficiently large vacuum layer (>10 Å) was added along the two directions perpendicular to the direction of supramolecular chain in order to avoid spurious interactions between the periodic images of the system. The resulting a lattice constant was 20 Å. The lattice constant c was varied between 20 Å for monomeric **1** to 40 Å for the heptamer. The dimensions of the periodic box were chosen such that the electron density approached zero at the cell border. Convergence with respect to the box size and the number of plane waves was explicitly tested in each case (see the Supporting Information). In the PW-DFT calculations performed on infinite chains of **1**, a dimer of BTA monomer **1** was placed in an ($a \times a \times c$) orthorhombic supercell. As in the case of oligomeric BTAs, for the periodic BTA chain, the cell parameter a was set to 20 Å to ensure a sufficient vacuum layer of >10 Å between the supramolecular chains in neighboring periodic images of the system to avoid spurious interactions between them. Optimum lattice constants c equal to 7.36 Å were chosen from the minimization of the total energy with respect to this parameter.[66] It should be noted that PW-DFT is inherently free of basis set superposition error (BSSE), because plane-wave basis sets describe any point in the periodic supercell with the same quality, in contrast to Gaussian orbitals spanning only a local region.[67]

Parallel to the PW-DFT electronic structure calculations, molecular orbital calculations using Gaussian-type orbitals (GTOs) were performed on the monomer and oligomers of **1** using the Gaussian 03 suite of programs[68] with the same exchange-correlation functional (PBE) and the 6-31G(d,p) split-valence basis set. To account for the BSSE, optimization on a counterpoise-corrected potential energy surface (PES) was performed. However, because of the very high computational demands associated with the application of such a methodology to extensive molecular models, the GTO−DFT calculations in this study were limited to BTA oligomeric models up to and including the tetramer.

Full geometry optimization was performed on all models without any symmetrical constraints. The nature of the stationary points was evaluated from the harmonic modes, computed either analytically using Gaussian or numerically using VASP, using a complete Hessian matrix for all models. No imaginary frequencies were found for the optimized structures in Gaussian, confirming that these geometries correspond to local minima on the potential energy surface. In the case of PW-DFT, all frequencies were real except for some low-frequency imaginary vibrations (less than 30 cm^{-1}). Several attempts were made to remove these imaginary frequencies by using slightly different geometries obtained by perturbation of the geometries along the eigenvectors corresponding to these vibrations. No reduction of imaginary frequencies was achieved, indicating a very shallow potential energy surface.

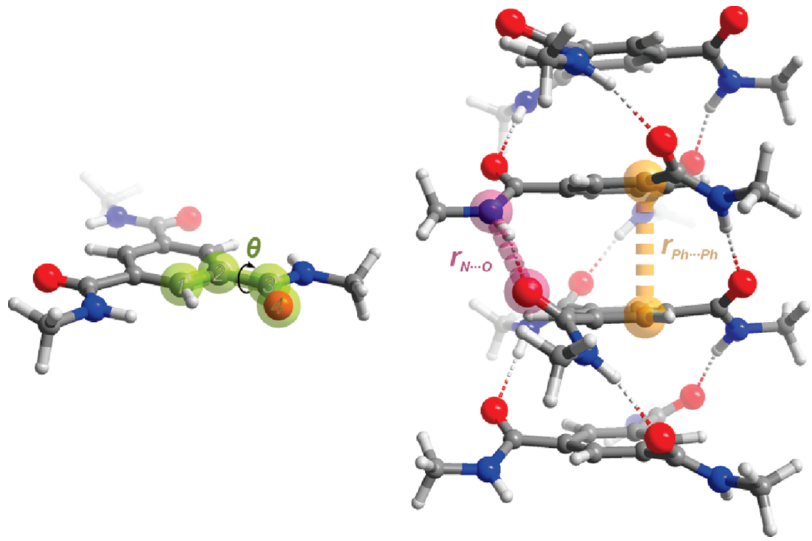

Figure 2. Key geometric parameters of BTA mono- and oligomeric systems used for the comparison of the theoretical and experimental results: the dihedral angle (θ) as the extent of the nonplanarity of the carbonyl-amide group relative to the benzene ring; the H-bond distance ($r_{N\cdots O}$) measured as the distance between the nitrogen and oxygen atoms; and the inter-ring centroid distance ($r_{Ph\cdots Ph}$), defined as the distance between the center of one benzene ring and the center of the benzene ring adjacent to it.

To estimate stabilities and interaction energies within different BTA supramolecular aggregates, electronic DFT-computed energies were used. We also considered the respective zero-point-energy- (ZPE-) corrected energies and enthalpies for the estimation of these parameters (see the Supporting Information). It was found that the correction of the electronic energies with ZPE (E_{ZPE}) and finite-temperature terms (H_{CORR}) did not lead to any qualitative changes in the observed trends. Only a rather uniform shift of 10−14 kJ/mol in the average interaction ZPE-corrected energies as well as enthalpies within BTA stacks containing two to four monomers was observed. Because of the computational limitations, the frequency analysis required for computing H_{CORR} and E_{ZPE} was performed only for BTA aggregates with one to four monomers. Therefore, to ensure an adequate comparison of different energy values for different supramolecular aggregates considered herein, we limit the discussion to only those values derived from electronic DFT-computed energies.

From the calculated electronic energies of the n-mers, the average interaction energy was calculated by subtracting n times the energy of the monomer from the energy of the oligomer and dividing this value by the number of intermolecular interactions

$$\Delta E_{avg} = (E_n - nE_1)/(n - 1) \quad (1)$$

Electron-density difference maps for each BTA oligomer were obtained by subtracting the sum of the total electron densities of the constituent monomers obtained by PW-DFT calculations (using their geometries in the bonded complex) from the total electron density of the hydrogen-bonded BTA oligomer obtained using the same method. Moreover, the same procedure was applied to obtain the electron-density difference of a hexamer from its two constituting trimers. The open-source visualization program OpenDX[69] was used to plot the difference in densities, $\Delta\rho$, on a plane in which the oxygen and hydrogen atoms of two neighboring BTA units are located. The electrostatic potential surface for each BTA oligomer was calculated using PW-DFT and visualized using the above-mentioned software on an isodensity surface corresponding to an electron density of 10^{-5} electrons/Å^3.

Results and Discussion

Structure Validation. Before attempting to rationalize the cooperative interactions in hydrogen-bonded BTA oligomers, we first validated our approach by comparing the PW-DFT-obtained geometries of **1** with reported crystal structures of several BTA derivatives. Three important geometrical parameters, namely, (1) the dihedral angle, (2) the H-bond distance, and (3) the inter-ring centroid distance (Figure 2), in the optimized geometry of the infinite BTA chain of **1** were compared with the values observed in the crystal structures reported by Lightfoot et al.[70] (**2a**, Figure 3a), Ranganathan et al.[71] (**2b**, Figure 3b), and Gong et al.[72] (**2c**, Figure 3c). In all reported crystal structures, BTA monomers are stacked onto each other through threefold hydrogen bonding.

A comparison between the optimized geometry of the infinite BTA chain of **1** and the reported crystal structures is presented in Table 1. Although the side chains of BTA monomers **2a** and **2b** contain hydrogen-bond acceptors, it can be seen that both the dihedral angle and the hydrogen-bond lengths are in close agreement with the optimized geometry of the infinite BTA chain of **1** having only a methyl group as a side chain. However, the difference in inter-ring centroid distance between optimized geometry and reported crystal structures is somewhat larger.

These results suggest that the columnar packing observed in the crystal structures of **2a** and **2b** is not influenced by competitive hydrogen bonding due to the presence of hydrogen-bond acceptors in their side chains. However, the key geometrical parameters of the crystal structure of BTA **2c** differ substantially from the reported crystal structures of BTAs **2a** and **2b** and from the optimized geometry of the infinite chain of BTA **1** because the terminal acid group in the side chain of **2c** competes with the intermolecular amide hydrogen bonding between the BTA units in the columnar stack. This competition results in a smaller dihedral angle and a substantially larger intermolecular hydrogen-bond length. A similar competition effect was recently reported by Rochefort and co-workers in

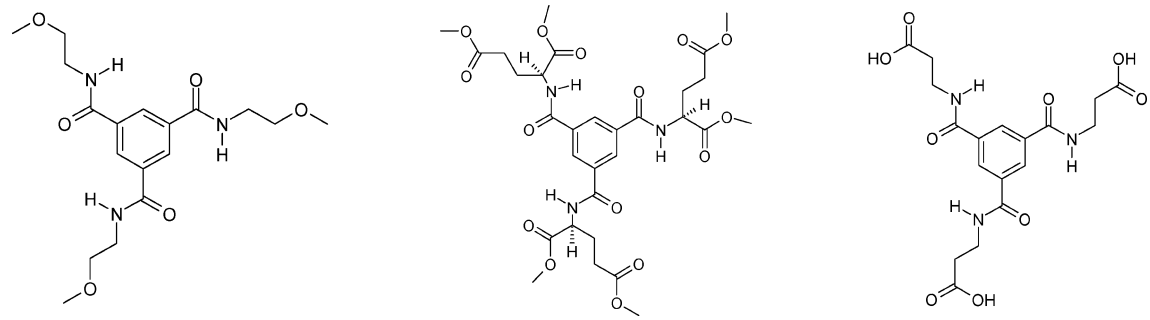

2a (a) 2b (b) 2c (c)

Figure 3. Molecular structure of BTA monomers and reference to reported crystal structures: (a) **2a**, Lightfoot et al.;[70] (b) **2b**, Ranganathan et al.;[71] and (c) **2c**, Gong et al.[72]

TABLE 1: Comparison of the Dihedral Angle, Inter-Ring Centroid Distance, and H-Bond Distance between the PW-DFT-Optimized Geometry of the Infinite Chain of 1 and Crystal Structures of Several BTA Molecules Reported by Lightfoot et al.[70] (2a), Ranganathan et al.[71] (2b), and Gong et al.[72] (2c)

	dihedral angle (deg)	$r_{Ph\cdots Ph}$ (Å)	$r_{N\cdots O}$ (Å)
PW-DFT infinite chain of BTA **1**	40.5	3.68	2.95
2a[70]	41.5	3.62	2.97
2b[71]	40.2	3.63	2.95
2c[72]	21.4	3.66	3.84

TABLE 2: Binding Energies (ΔE_{dim}), Distances between the Phenyl Rings ($r_{Ph\cdots Ph}$), and H-Bond Distances ($r_{N\cdots O}$) of a Dimer of 1 Calculated Using the PBE functional with a PW Basis Set or a GTO-Type Basis Set

	ΔE_{dim} (kJ/mol)	$r_{Ph\cdots Ph}$ (Å)	$r_{N\cdots O}$ (Å)
E-PW 400 eV	−39	3.57	3.05
E-GTO	−72	3.72	3.01
E-GTO-cp-sp[a]	−26	3.72	3.01
E-GTO-cp-opt[b]	−36	3.50	3.09

[a] GTO calculation with counterpoise correction using single-point modification of the interaction energy. [b] GTO calculation using a counterpoise-corrected PES.

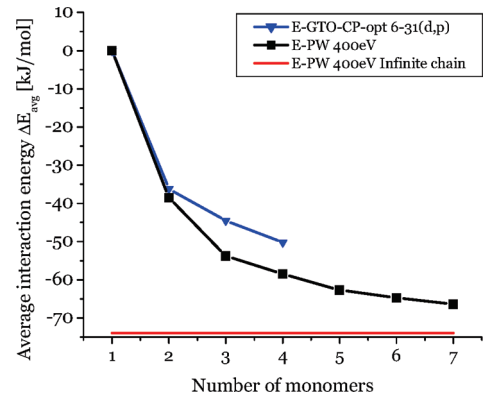

Figure 4. Calculated average electronic interaction energy of BTA oligomers as a function of oligomer size obtained by (1) GTOs on a counterpoise- (CP-) corrected potential energy surface (PES) (blue triangles), (2) PW (black squares), and (3) PW infinite chain (red line).

their DFT study on BTA oligomers substituted with additional hydrogen-bonding donors and acceptors at the 2, 4, and 6 positions.[73]

Cooperativity in the Supramolecular Polymerization of Trialkylbenzene-1,3,5-tricarboxamides. Having justified the PW-DFT-obtained geometries by comparison with reported crystal structures, we next investigated the origin of the cooperative growth of BTA-based supramolecular polymers. Electronic structure calculations were performed to understand and quantify the experimentally observed cooperative growth of BTA-based supramolecular polymers. Table 2 summarizes the interaction energies and key geometric parameters obtained by the various methods investigated for a BTA dimer consisting of **1**. First, it can be concluded that BSSE results in a substantial overestimation of the intermolecular interaction energy (i.e., the interaction energy of a dimer becomes more negative). Upon application of a counterpoise correction (CP) to the GTO calculations of the dimer, the interaction energy within a dimer is significantly decreased. We evaluated two methods for applying CP corrections to the GTO calculations of the BTA dimer. In the first method, CP-corrected energies were obtained using single-point modification of the interaction energy of a BTA dimer. In the second method, CP corrections were considered on the whole potential energy surface (PES). Comparison of the interaction energies and geometrical parameters obtained by these two methods with those obtained by PW-DFT, which is inherently free from BSSE, shows that CP should be used to correct both the optimized geometry and the interaction energy. Thus, to avoid the impact of BSSE on the GTO calculations, geometry optimizations of BTA oligomeric models were performed on a CP-corrected PES.

Figure 4 displays the calculated average electronic interaction energy as a function of chain length obtained from the GTO calculations on a CP-corrected PES for BTA oligomers containing two to four monomers of **1**, as well as from PW calculations of BTA oligomers containing two to seven monomers of **1**. As a limiting case for BTA supramolecular structures, we calculated the average interaction energy per monomer in an infinite chain using PW-DFT with a box size of $20 \times 20 \times 7.36$ Å^3 (depicted as the red line in Figure 4) and periodic boundary conditions. From the data in Figure 4, it can be seen that the average interaction strength increases with the number of monomers, indicating that the formation of larger oligomers is energetically increasingly favorable with respect to the formation of smaller oligomers. The average interaction energy slowly decreases toward the asymptotic value of the infinite chain. The calculated average interaction energy obtained for the heptamer (−66 kJ/

TABLE 3: PW-DFT PBE Electronic Energies (ΔE_{nk}, kJ/mol) of Threefold Hydrogen Bonds As a Function of Chain Length (n) and Position within the Stack (k)

	k		
n	1	2	3
2	−38.7		
3	−69.3		
4	−68.4	−99.0	
5	−75.8	−105	
6	−72.9	−110	−109
7	−75.4	−110	−116

mol) is already close to the value for the infinite BTA chain (−74 kJ/mol).

To rationalize the origin of the cooperative effect operating in larger BTA oligomers, the interaction energies were analyzed using the methodology previously applied by Dannenberg et al.[31] to describe hydrogen-bond cooperativity in formamide oligomers. Within this approach, the energies of the individual interactions between specific subunits of lengths i and j of a supramolecular ensemble are calculated by taking the difference between the total energy of an optimized oligomer containing n monomeric units and subtracting the energies of two smaller optimized oligomers of lengths i and j where $i+j = n$. We assume symmetrical interactions within BTA oligomers, that is, breaking bonds that are the same distance from either end of the stack to form the same two smaller fragments requires equivalent energies. Thus, Table 3 contains only entries for breaking hydrogen bonds starting at one end up to and including the most central threefold hydrogen-bonding interaction.

The data summarized in Table 3 indicate that the local interactions become stronger as the BTA oligomer becomes larger (i.e., the interaction of a monomer and a hexamer in a heptamer is −75.4 kJ/mol as compared to −69.3 kJ/mol for the interaction of a monomer and a dimer in a trimer). Furthermore, interactions close to the interior of a BTA oligomer are stronger than those near the edges of the chain (i.e., the interaction energy of the central bond in a hexamer is −109 kJ/mol, whereas that at the edge is only −72.9 kJ/mol). Among the data points considered, the weakest interaction is that in the BTA dimer (−38.7 kJ/mol), and the strongest is the central interaction ($k = 3$) in the BTA oligomer containing seven monomers (−116 kJ/mol). Thus, the strongest interaction is 3 times stronger than that of the dimer. Therefore, there is an overall cooperative effect of 200%. As can be seen from Figure 5, the increase in interaction strength is accompanied by a reduction in the average hydrogen-bond length. Such a feature has been also observed in computational studies on the cooperative formation of hydrogen-bonded formamide chains.[30]

The total cooperativity can be decomposed into (1) pairwise electrostatic interactions (mainly long-range dipole−dipole interactions), (2) nonpairwise short-range (mutual) polarization, and (3) resonance-assisted hydrogen bonding.[31−33] To estimate the contribution of the electrostatic interactions on the total cooperativity, we applied a pairwise dipole−dipole model (see the Supporting Information).[31] The long-range dipole−dipole interactions are proportional to $1/R^3$, where R is the distance between the dipoles. Under the assumption that N dipoles are linearly aligned and evenly spaced, the maximum cooperative long-range dipole−dipole interaction for the strongest bond in the chain consisting of seven BTA monomers would be 43%. This would leave 157% due to polarization and/or resonance-assisted hydrogen bonding.

The analysis presented above holds only under the assumption that, upon growth of the supramolecular polymer, the geometrical and, rather related, electronic properties of the involved molecular species remain unchanged, as is the case for one-dimensional hydrogen-bonded oligomers formed from relatively small and stiff molecules such as formamide. In contrast, for the supramolecular polymers formed from BTAs, the situation is more complex. Indeed, the geometry of BTA monomeric units within oligomeric and polymeric chains is significantly perturbed as compared to that in the monomeric state. This has a large impact on the electronic properties and, consequently, on the strength and behavior of the respective intermolecular interactions within the resulting macromolecules.

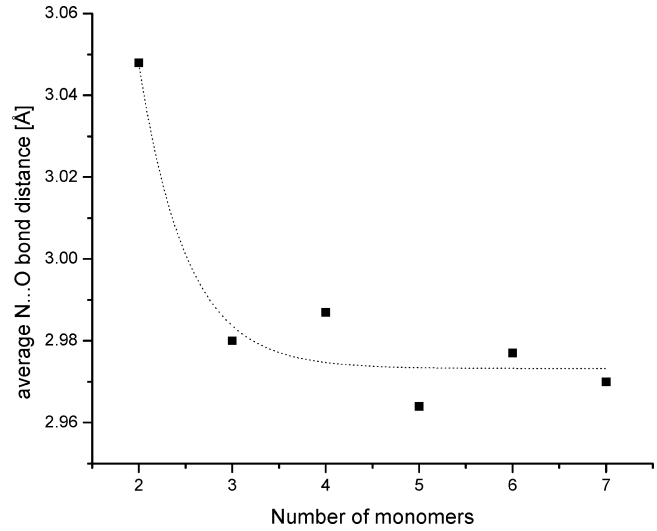

Figure 5. Average N···O H-bond distances as a function of the number of monomers in the BTA oligomer. The dotted line is provided to guide the eyes.

Upon self-assembly of BTA monomers into a supramolecular polymer, the amide group of the monomeric unit rotates out of the plane of the benzene ring. Whereas the dihedral angle, θ (Figure 2), in the optimized geometry of the infinite chain of **1** equals 40°, it is only 12° in the optimized structure of monomeric **1**.[66] Such a deformation shifts the structure considerably from its equilibrium geometry and contributes unfavorably to the overall interaction energy due to the fact that conjugation of the carbonyl group with the aromatic benzene ring is diminished. To account for the energy loss associated with such deformations, we recalculated the binding energy of the strongest bond in the heptamer ($k = 3$) by subtracting from the electronic energy of the optimized structure of the BTA heptamer the electronic energies of the trimer and tetramer obtained by single-point calculations on the nonoptimized geometries of the respective subunits constituting the heptameric structure

$$\Delta E_{\mathrm{B}} = E_{n,\mathrm{opt}} - E_{i,\mathrm{sp}} - E_{n-i,\mathrm{sp}} \qquad (2)$$

where $E_{n,\mathrm{opt}}$ represents the electronic energy of an optimized n-mer, $E_{i,\mathrm{sp}}$ represents the electronic energy of a nonoptimized i-mer (with $i < n$) in which the monomeric repeating units have the same geometry as the monomeric repeating units in the larger n-mer, and $E_{n-i,\mathrm{sp}}$ represents the electronic energy of a nonoptimized oligomer of length $n - i$ in which the monomers have the same geometry as the monomers in the larger n-mer.

According to Table 4, when the unfavorable energies as a result of loss of conjugation of the BTA monomer upon inclusion in the chain are taken into account, the overall cooperative effect of hydrogen bonding in BTA chains reduces substantially (when BTA heptamers and dimers are compared,

TABLE 4: Electronic Interaction Energies for the Formation of a BTA Dimer and Central Bond in a BTA Heptamer with (ΔE_b) and without (ΔE_{nk}) Taking into Account Changes in Geometry As a Result of Incorporation of the BTA Monomer in a BTA Oligomer and Unfavorable Energy As a Result of the Geometrical Changes of the Monomer upon Inclusion in a Hydrogen-Bonded BTA Chain (ΔE_d)[a]

number of monomers, n	ΔE_{nk}	ΔE_b	ΔE_d[b]
2	−38.7	−70.2[c]	+31.5
7 ($k = 3$)	−116	−151	+35

[a] All energies are in kJ/mol. [b] Calculated as the difference between ΔE_{nk} and ΔE_b. [c] This value was computed by subtracting twice the electronic energy of a monomer having the same geometry as one of the two central monomers in the heptamer from the electronic energy of the central dimer in the heptamer.

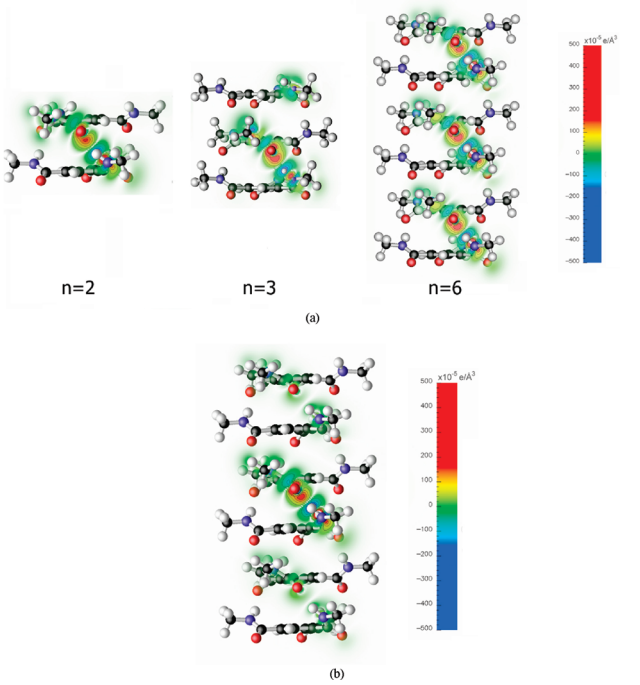

Figure 6. Electron-density differences calculated (a) by subtracting the electron density of the individual monomers from the electron density of the constituting oligomer (dimer, trimer, and hexamer) and (b) by subtracting the electron density of two trimers within a hexamer from the electron density of the constituting hexamer. Values are in electrons/Å^3. Red regions denote accumulation of electron density, and blue regions correspond to depletion of electron density upon formation of the hydrogen-bond complex.

the cooperativity reduces to only 114% as opposed to the above-mentioned 200%). Subtraction of the 43% due to the long-range pairwise dipole−dipole interactions results in 71% cooperativity due to polarization and/or resonance-assisted hydrogen bonding (RAHB), both effects leading to electron redistribution along the BTA chain.

The increase in hydrogen-bond strength due to redistribution of electron density along the BTA chain can be visualized by calculating the changes in electron density upon hydrogen bonding of the BTA monomers. The use of electron-density shifts is advantageous as it does not make use of atomic charges, the calculation of which requires arbitrary partitioning of the electron density to one atom or another.[74] Figure 6a displays the electron-density difference maps upon formation of a BTA oligomer from its constituting monomers. The main changes observed upon hydrogen bonding of the monomeric BTAs are

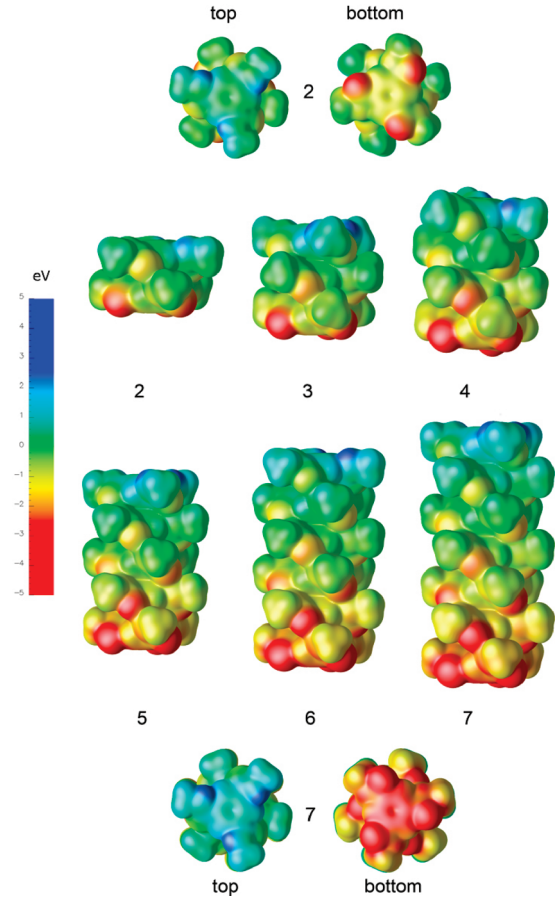

Figure 7. Electrostatic potential in eV, plotted on isodensity surfaces of 10^{-5} electrons/Å^3, for the dimer through the heptamer. Additionally, top and bottom views for the dimer and heptamer are plotted. Red colors denote regions that attract a positive charge, whereas blue colors denote regions that repel a positive charge. Within this representation, the carbonyl functionality points toward the bottom of the stack, and the amide functionality points toward the top.

the polarization of electron density within the hydrogen-bond acceptor toward regions where the acceptor lone pair is located, together with a polarization of the hydrogen-bond donor resulting in a decrease in electron density on the hydrogen-bond donor. Furthermore, it can be seen that the distance between the contour lines decreases as the BTA oligomer grows in length, indicating an increase in local polarization as the BTA oligomer becomes larger in size. Finally, to visualize the electron redistribution as a result of hydrogen-bond cooperativity as the BTA chain grows in length, the electron-density difference map at the central bond of a hexamer was calculated by extending the trimer to the hexamer (Figure 6b). As can be observed from Figure 6b, there is an increase in electron density around the oxygen and a decrease around the hydrogen with increasing chain length, resulting in stronger hydrogen bonds.

We also evaluated the electrostatic potential surface as a function of oligomer size (Figure 7). The electrostatic potential surfaces demonstrate that, in addition to a local polarization, an overall polarization over the whole hydrogen-bonded BTA chain is also present. The latter is a consequence of both the superposition principle of the dipole vectors of the individual monomers constituting the stack and electron redistribution as a result of hydrogen bonding. Comparison of the top and bottom monomers of the dimer and heptamer shows that the electrostatic potential of the top monomer of the heptamer is more negative than that of the top monomer of the dimer. Likewise, the bottom

monomer of the heptamer has a more positive electrostatic potential than the bottom monomer of the dimer. The images for the trimer up to and including the hexamer show that the overall polarization increases with increasing number of monomers. Experimental evidence for the overall polarization of BTA columns in the liquid-crystalline state was recently found in aligned BTA columns in thin films.[75]

The results of our computational study show that the cooperative growth of BTA oligomers is caused by electronic effects arising as a result of polarization of the hydrogen bonds as the oligomers grow larger in length. This indicates that it is possible to tune the average degree of polymerization at a given concentration by employing electron-donating and -accepting groups in the side chain, as the average degree of polymerization critically depends on cooperative effects.[15] This idea is partially supported by recent solid-state studies on BTA crystals in which the methyl group of **1** was replaced with a phenyl group, resulting in a large decrease in melting temperature as a result of weakening of the hydrogen bonds due to enhanced electron delocalization.[76] We hypothesize that the hydrogen-bond cooperativity in BTA-based supramolecular polymers will play a crucial role in determining emergent macroscopic material properties such as toughness, strength, and self-healing capabilities, as has recently been shown to be the case for protein nanofibrils.[77]

Summary and Outlook

Herein, we have carried out DFT calculations to understand the origin of the experimentally observed cooperativity in the hydrogen-bond-induced supramolecular polymerization of C_3-symmetrical trialkylbenzene-1,3,5-tricarboxamides (BTAs), a supramolecular motif used in various types of applications. In particular, we have shown that PW-DFT is an attractive method for theoretically investigating self-assembled structures as a result of the absence of the BSSE in PW-based calculations. Using the calculated PW electronic energies corrected for deformation of the monomer upon inclusion in the chain, we have shown that the central interaction (consisting of three amide hydrogen bonds) in a BTA heptamer is 114% energetically more favorable compared to formation of the same interaction in a BTA dimer. By applying a simple pairwise dipole−dipole model, we found that 43% could be attributed to long-range dipole−dipole interactions, leaving 71% as being due to polarization and/or resonance-assisted hydrogen bonding (RAHB). The electron-density redistributions occurring as a result of these nonadditive effects could be visualized by calculation of the electron-density difference maps, which indeed revealed significant changes in the local polarization around the amide hydrogen bond as the BTA chain grew larger in size.

Currently, theoretical efforts are underway to investigate the influence of side-chain length and chirality on the cooperative growth of BTA-based supramolecular polymers. Moreover, the DFT results on the BTA oligomers will be used to accurately calibrate force fields for use in molecular dynamics simulations, allowing for the prediction of emerging mechanical properties of BTA-based supramolecular materials. Understanding cooperativity in the growth of supramolecular polymers is a key step toward the rational design of 1D supramolecular structures across multiple length scales with defined function and composition.

Acknowledgment. We are grateful to Prof. Dr. E. W. Meijer for stimulating discussions. We also thank Dr. A. P. J. Jansen for his insightful comments. The National Computing Facilities Foundation (NCF) is acknowledged for providing computational resources, with financial support from NWO (SH-125-08).

Supporting Information Available: Optimized Cartesian coordinates of the investigated BTA monomer and oligomers, evaluation of the effect of box size and cutoff energy in the VASP calculations, calculation of the energetic stabilization as a result of pairwise dipole−dipole interactions, and contribution of ZPE and finite-temperature corrections to the average interaction energy. This material is available free of charge via the Internet at http://pubs.acs.org.

References and Notes

(1) Hartgerink, J. D.; Beniash, E.; Stupp, S. I. *Science* **2002**, *99*, 5133.
(2) Palmer, L. C.; Stupp, S. I. *Acc. Chem. Res.* **2008**, *41*, 1674.
(3) Müller, M.; Brunsveld, L. *Angew. Chem., Int. Ed.* **2009**, *48*, 2921.
(4) Zang, L.; Che, Y.; Moore, J. S. *Acc. Chem. Res.* **2008**, *41*, 1596.
(5) Chen, Z.; Lohr, A.; Saha-Möller, C. R.; Würthner, F. *Chem. Soc. Rev.* **2009**, *38*, 564.
(6) Lee, C. C.; Grenier, C.; Meijer, E. W.; Schenning, A. P. H. J. *Chem. Soc. Rev.* **2009**, *38*, 671.
(7) Takazawa, K.; Kitahama, Y.; Kimura, Y.; Kido, G. *Nano Lett.* **2005**, *5*, 1293.
(8) Hak Oh, J.; Woo Lee, H.; Mannsfeld, S.; Stoltenberg, R. M.; Jung, E.; Wan Jin, Y.; Min Kim, J.; Yoo, J.-B.; Bao, Z. *Proc. Natl. Acad. Sci. U.S.A.* **2009**, *106*, 6065.
(9) Yamamoto, Y.; Fukushima, T.; Suna, Y.; Ishii, N.; Saeki, A.; Seki, S.; Tagawa, S.; Taniguchi, M.; Kawai, T.; Aida, T. *Science* **2006**, *314*, 1761.
(10) Douglas, J. F. *Langmuir* **2009**, *25*, 8386.
(11) Elemans, J. A. A. W.; Rowan, A. E.; Nolte, R. J. M. *J. Mater. Chem.* **2003**, *13*, 2661.
(12) Dudowicz, J.; Douglas, J. F.; Freed, K. F. *J. Chem. Phys.* **2009**, *130*, 224906.
(13) Aggeli, A.; Nyrkova, I. A.; Bell, M.; Harding, R.; Carrick, L.; McLeish, T. C. B.; Semenov, A. N.; Boden, N. *Proc. Natl. Acad. Sci. U.S.A.* **2001**, *98*, 11857.
(14) Zayed, J. M.; Nouvel, N.; Rauwald, U.; Scherman, O. A. *Chem. Soc. Rev.* **2010**, *39*, 2806.
(15) de Greef, T. F. A.; Smulders, M. M. J.; Wolffs, M.; Schenning, A. P. H. J.; Sijbesma, R. P.; Meijer, E. W. *Chem. Rev.* **2009**, *109*, 5687.
(16) de Greef, T. F. A.; Meijer, E. W. *Nature* **2008**, *453*, 171.
(17) Hunter, C. A.; Anderson, H. L. *Angew. Chem., Int. Ed.* **2009**, *48*, 7488.
(18) Jeffrey, G. A.; Saenger, W. *Hydrogen Bonding in Biological Structures*; Springer-Verlag: Berlin, 1991.
(19) Scheiner, S. *Hydrogen Bonding*; Oxford University Press: New York, 1997.
(20) Çarçabal, P.; Jockusch, R. A.; Hünig, I.; Snoek, L. C.; Kroemer, R. T.; Davis, B. G.; Gamblin, D. P.; Compagnon, I.; Oomens, J.; Simons, J. P. *J. Am. Chem. Soc.* **2005**, *127*, 11414.
(21) DeChancie, J.; Houk, K. N. *J. Am. Chem. Soc.* **2007**, *129*, 5419.
(22) Otero, R.; Schöck, M.; Molina, L. M.; Lægsgaard, E.; Stensgaard, I.; Hammer, B.; Besenbacher, F. *Angew. Chem., Int. Ed.* **2005**, *117*, 2310.
(23) van Mourik, T.; Dingley, A. J. *J. Phys. Chem. A* **2007**, *111*, 11350.
(24) Wu, Y.-D.; Zhao, Y.-L. *J. Am. Chem. Soc.* **2001**, *123*.
(25) Parra, R. D.; Ohlssen, J. *J. Phys. Chem. A* **2008**, *112*, 3492.
(26) Rossetti, G.; Magistrato, A.; Pastore, A.; Carloni, P. *J. Chem. Theory Comput.* **2010**, *6*, 1777.
(27) Suh, S. B.; Kim, J. C.; Choi, Y. C.; Yun, S.; Kim, K. S. *J. Am. Chem. Soc.* **2004**, *126*, 2186.
(28) Dannenberg, J. J.; Haskamp, L.; Masunov, A. *J. Phys. Chem. A* **1999**, *103*, 7083.
(29) Masunov, A.; Dannenberg, J. J. *J. Phys. Chem. B* **2000**, *104*, 806.
(30) Kobko, N.; Paraskevas, L.; del Rio, E.; Dannenberg, J. J. *J. Am. Chem. Soc.* **2001**, *123*, 4348.
(31) Kobko, N.; Dannenberg, J. J. *J. Phys. Chem. A* **2003**, *107*, 10389.
(32) Gilli, G.; Bellucci, F.; Ferretti, V.; Bertolasi, V. *J. Am. Chem. Soc.* **1989**, *111*, 1023.
(33) Bertolasi, V.; Gilli, P.; Ferretti, V.; Gilli, G. *J. Am. Chem. Soc.* **1991**, *113*, 4917.
(34) Morozov, A. V.; Tsemekhman, K.; Baker, D. *J. Phys. Chem. B.* **2006**, *110*, 4503.
(35) Smulders, M. M. J.; Nieuwenhuizen, M. M. L.; de Greef, T. F. A.; van der Schoot, P.; Schenning, A. P. H. J.; Meijer, E. W. *Chem.—Eur. J.* **2010**, *16*, 362.
(36) Hanabusa, K.; Kawamaki, A.; Kimura, M.; Shirai, H. *Chem. Lett.* **1997**, 191.
(37) Hanabusa, K.; Koto, C.; Kimura, M.; Shirai, H.; Kakehi, A. *Chem. Lett.* **1997**, 492.

(38) Ogata, D.; Shikata, T.; Hanabusa, K. *J. Phys. Chem. B* **2004**, *108*, 15503.
(39) Smulders, M. M. J.; Schenning, A. P. H. J.; Meijer, E. W. *J. Am. Chem. Soc.* **2008**, *130*, 606.
(40) Douglas, J. F.; Dudowicz, J.; Freed, K. F. *J. Chem. Phys.* **2008**, *128*, 224901.
(41) Jonkheijm, P.; van der Schoot, P.; Schenning, A. P. H. J.; Meijer, E. W. *Science* **2006**, *313*, 80.
(42) Roosma, J.; Mes, T.; Leclère, P.; Palmans, A. R. A.; Meijer, E. W. *J. Am. Chem. Soc.* **2008**, *130*, 1120.
(43) de Loos, M.; van Esch, J. H.; Kellogg, R. M.; Feringa, B. L. *Tetrahedron* **2007**, *63*, 7285.
(44) Yasuda, Y.; Iishi, E.; Inada, H.; Shirota, Y. *Chem. Lett.* **1996**, *7*, 575.
(45) Matsunaga, Y.; Miyajima, N.; Nakayasu, Y.; Sakai, S.; Yonenaga, M. *Bull. Chem. Soc. Jpn.* **1988**, *61*, 207.
(46) Blomenhofer, M.; Ganzleben, S.; Hanft, D.; Schmidt, H.-W.; Kristiansen, M.; Smith, P.; Stoll, K.; Mäder, D.; Hoffmann, K. *Macromolecules* **2005**, *38*, 3688.
(47) Kresse, G.; Furthmüller, J. *Phys. Rev. B* **1996**, *54*, 11169.
(48) Kresse, G.; Hafner, J. *Phys Rev. B* **1993**, *47*, R558.
(49) Perdew, J. P.; Burke, K.; Ernzerhof, M. *Phys. Rev. Lett.* **1996**, *77*, 3865.
(50) Blöchl, P. E. *Phys. Rev. B* **1994**, *50*, 17953.
(51) Kresse, G.; Joubert, J. *Phys. Rev. B* **1999**, *59*, 1758.
(52) Ireta, J.; Neugebauer, J.; Scheffler, M. *J. Phys. Chem. A* **2004**, *108*, 5692.
(53) Ireta, J.; Neugebauer, J.; Scheffler, M.; Rojo, A.; Galván, M. *J. Phys. Chem. B* **2003**, *107*, 1432.
(54) Tuma, C.; Boese, A. D.; Handy, N. C. *Phys. Chem. Chem. Phys.* **1999**, *1*, 3939.
(55) Kaschner, R.; Hohl, D. *J. Phys. Chem. A* **1998**, *102*, 5111.
(56) van der Wijst, T.; Guerra, C. F.; Swart, M.; Bickelhaupt, F. M. *Chem. Phys. Lett.* **2006**, *426*, 415.
(57) Hamann, D. R. *Phys. Rev. B* **1997**, *55*, R10157.
(58) Frey, J. A.; Leutwyler, S. *J. Phys. Chem. A* **2006**, *110*, 12512.
(59) Zhao, Y.; Truhlar, D. G. *J. Chem. Theory Comput.* **2007**, *3*, 289.
(60) Morozov, A.; Kortemme, T.; Tsemekhman, K.; Baker, D. *Proc. Natl. Acad. Sci. U.S.A.* **2004**, *101*, 6946.
(61) Dobson, J. F.; Vignale, G.; Das, M. P. *Electronic Density Functional Theory: Recent Progress and New Directions*; Plenum: New York, 1997.
(62) Sinnokrot, M. O.; Sherrill, C. D. *J. Phys. Chem. A* **2006**, *110*, 10656.
(63) Grimme, S.; Antony, J.; Schwabe, T.; Mück-Lichtenfeld, C. *Org. Biomol. Chem.* **2007**, *5*, 741.
(64) Arey, J. S.; Aeberhard, P. C.; Lin, I. C.; Rothlisberger, U. *J. Phys. Chem. B* **2009**, *113*, 4726.
(65) Tauer, T. P.; Sherrill, C. D. *J. Phys. Chem. A* **2005**, *109*, 10475.
(66) Stals, P. J. M.; Everts, J. C.; de Bruijn, R.; Filot, I. A. W.; Smulders, M. M. J.; Martín-Rapún, R.; Pidko, E. A.; de Greef, T. F. A.; Palmans, A. R. A.; Meijer, E. W. *Chem.—Eur. J.* **2010**, *16*, 810.
(67) Fellers, R. S.; Barsky, D.; Gygi, F.; Colvin, M. *Chem. Phys. Lett.* **1999**, *312*, 548.
(68) Frisch, M. J.; Trucks, G. W.; Schlegel, H. B.; Scuseria, G. E.; Robb, M. R. E.; Cheeseman, J. R.; Montgomery, J. A., Jr.; Vreven, T.; Kudin, K. N.; Burant, J. C.; Millan, J. M.; Iyengar, S. S.; Tomasi, J.; Barone, V.; Mennucci, B.; Cossi, M.; Scalmani, G.; Rega, N.; Petersson, G. A.; Nakatsuji, H.; Hada, M.; Ehara, M.; Toyota, K.; Fukuda, R.; Hasegawa, J.; Ishida, M.; Nakajima, T.; Honda, Y.; Kitao, O.; Nakai, H.; Klene, M.; Li, X.; Knox, J. E.; Hratchian, H. P.; Cross, J. B.; Bakken, V.; Adamo, C.; Jaramillo, J.; Gomperts, R.; Stratmann, R. E.; Yazyev, O.; Austin, A. J.; Cammi, R.; Pomelli, C.; Ochterski, J. W.; Ayala, P. Y.; Morokuma, J.; Voth, G. A.; Salvador, P.; Dannenberg, J. J.; Zakrzewski, V. G.; Dapprich, S.; Daniels, A. D.; Strain, M. C.; Farkas, O.; Malick, D. K.; Rabuck, A. D.; Raghavachari, K.; Foresman, J. B.; Ortiz, J. V.; Cui, Q.; Baboul, A. G.; Clifford, S.; Cioslowski, J.; Stefanov, B. B.; Liu, G.; Liashenko, A.; Piskorz, P.; Komaromi, I.; Martin, R. L.; Fox, D. J.; Keith, T.; Al-Laham, M. A.; Peng, C. Y.; Nanayakkara, A.; Challacombe, M.; Gill, P. M. W.; Johnson, B.; Chen, W.; Wong, M. W.; Gonzalez, C.; Pople, J. A. *Gaussian 03*; version D.01; Gaussian Inc.: Wallingford, CT, 2004.
(69) *OpenDX: The Open Source Software Project Based on IBM's Visualization Data Explorer*; IBM: Armonk, NY, 1999.
(70) Lightfoot, M. P.; Mair, F. S.; Pritchard, R. G.; Warren, J. E. *Chem. Commun.* **1999**, 1945.
(71) Ranganathan, D.; Kurur, S.; Gilardi, R.; Karle, I. L. *Biopolymers* **2000**, *54*, 289.
(72) Gong, B.; Zheng, C.; Yan, Y. *J. Chem. Cryst.* **1999**, *29*, 649.
(73) Rochefort, A.; Bayard, E.; Hadj-Messaoud, S. *Adv. Mater.* **2007**, *19*, 1992.
(74) Scheiner, S.; Kar, T. *J. Phys. Chem. A* **2002**, *106*, 1784.
(75) Fitié, C. F. C.; Roelofs, W. S. C.; Kemerink, M.; Sijbesma, R. P. *J. Am. Chem. Soc.* **2010**, *132*, 6892.
(76) Kristiansen, M.; Smith, P.; Chanzy, H.; Baerlocher, C.; Gramlich, V.; McCusker, L.; Weber, T.; Pattison, P.; Blomenhofer, M.; Schmidt, H.-W. *Cryst. Growth Des.* **2009**, *9*, 2556.
(77) Keten, S.; Xu, Z.; Ihle, B.; Buehler, M. J. *Nat. Mater.* **2010**, *9*, 359.

JP1072928